nature geoscience

Article

https://doi.org/10.1038/s41561-024-01541-y

# Marine carbon sink dominated by biological pump after temperature overshoot

Received: 2 February 2024

Accepted: 22 August 2024

Published online: 30 September 2024

Check for updates

Wolfgang Koeve[1] ✉, Angela Landolfi[2], Andreas Oschlies[1] & Ivy Frenger[1] ✉

In the event of insufficient mitigation efforts, net-negative $CO_2$ emissions may be required to return climate warming to acceptable limits as defined by the Paris Agreement. The ocean acts as an important carbon sink under increasing atmospheric $CO_2$ levels when the physico-chemical uptake of carbon dominates. However, the processes that govern the marine carbon sink under net-negative $CO_2$ emission regimes are unclear. Here we assessed changes in marine $CO_2$ uptake and storage mechanisms under a range of idealized temperature-overshoot scenarios using an Earth system model of intermediate complexity over centennial timescales. We show that while the fate of $CO_2$ from physico-chemical uptake is very sensitive to future atmospheric boundary conditions and $CO_2$ is partly lost from the ocean at times of net-negative $CO_2$ emissions, storage associated with the biological carbon pump continues to increase and may even dominate marine excess $CO_2$ storage on multi-centennial timescales. Our findings imply that excess carbon that is attributable to the biological carbon pump needs to be considered carefully when quantifying and projecting changes in the marine carbon sink.

Under rising carbon dioxide ($CO_2$) emissions since pre-industrial times, the ocean has been an important sink of anthropogenic $CO_2$, thereby reducing potential global warming. In recent decades, the marine $CO_2$ sink has been equivalent to about 25% of emissions from fossil fuel burning, cement production and land use change, and has largely been rising in proportion to the rise in atmospheric $CO_2$ (refs. 1–3). The marine $CO_2$ sink is largely due to physical–chemical processes associated with the anthropogenically perturbed atmosphere–ocean $CO_2$ partial pressure ($p_{CO_2}$) gradient and seawater $CO_2$ buffer chemistry, while the net effect of physical and biogeochemical feedbacks under a changing climate, the so-called 'carbon–climate feedbacks', is usually considered to be relatively small[3–6].

In particular, changes in the biological carbon pump[7] (see 'Carbon pump terminology' in the Methods)—as one potential carbon–climate feedback process—are thought to be of limited importance for the additional uptake of atmospheric $CO_2$ by the ocean under rising atmospheric $p_{CO_2}$ ($p_{CO_2^{atm}}$) and on decadal timescales (for example, 2% for the time period 1995–2018[8]), which is in contrast to its important control of atmospheric carbon on long timescales (for example, glacial–interglacial)[9]. This is the case because a global decrease in the storage of carbon that is attributable to the biological carbon pump (termed 'biological pump carbon' throughout), which is driven by a declining export of organic matter into the interior ocean[10–12], is projected to be overcompensated by an increase in the biological-pump carbon in the interior ocean that is driven by increasing ocean residence times by the end of this century[13–17].

Limiting global warming to an acceptable degree[18] is very likely to require net-negative $CO_2$ emissions after some overshoot of surface air temperature (SAT), to compensate for too-high greenhouse gas emissions before reaching the peak SAT[19,20]. Net-negative $CO_2$ emissions imply substantially declining atmospheric $CO_2$ boundary conditions that may also be accompanied by the ocean transitioning from a net sink to a source of $CO_2$ into the atmosphere after the overshoot[21–24]. However, the response and relative role of different marine carbon sinks (the physico-chemical 'solubility' pump versus the biological carbon pump) under such conditions is currently not well understood.

[1]Biogeochemical Modelling, GEOMAR Helmholtz Centre for Ocean Research Kiel, Kiel, Germany. [2]National Research Council of Italy, Institute of Marine Sciences (CNR-ISMAR), Rome, Italy. ✉e-mail: wkoeve@geomar.de; ifrenger@geomar.de

https://doi.org/10.1038/s41561-024-01541-y

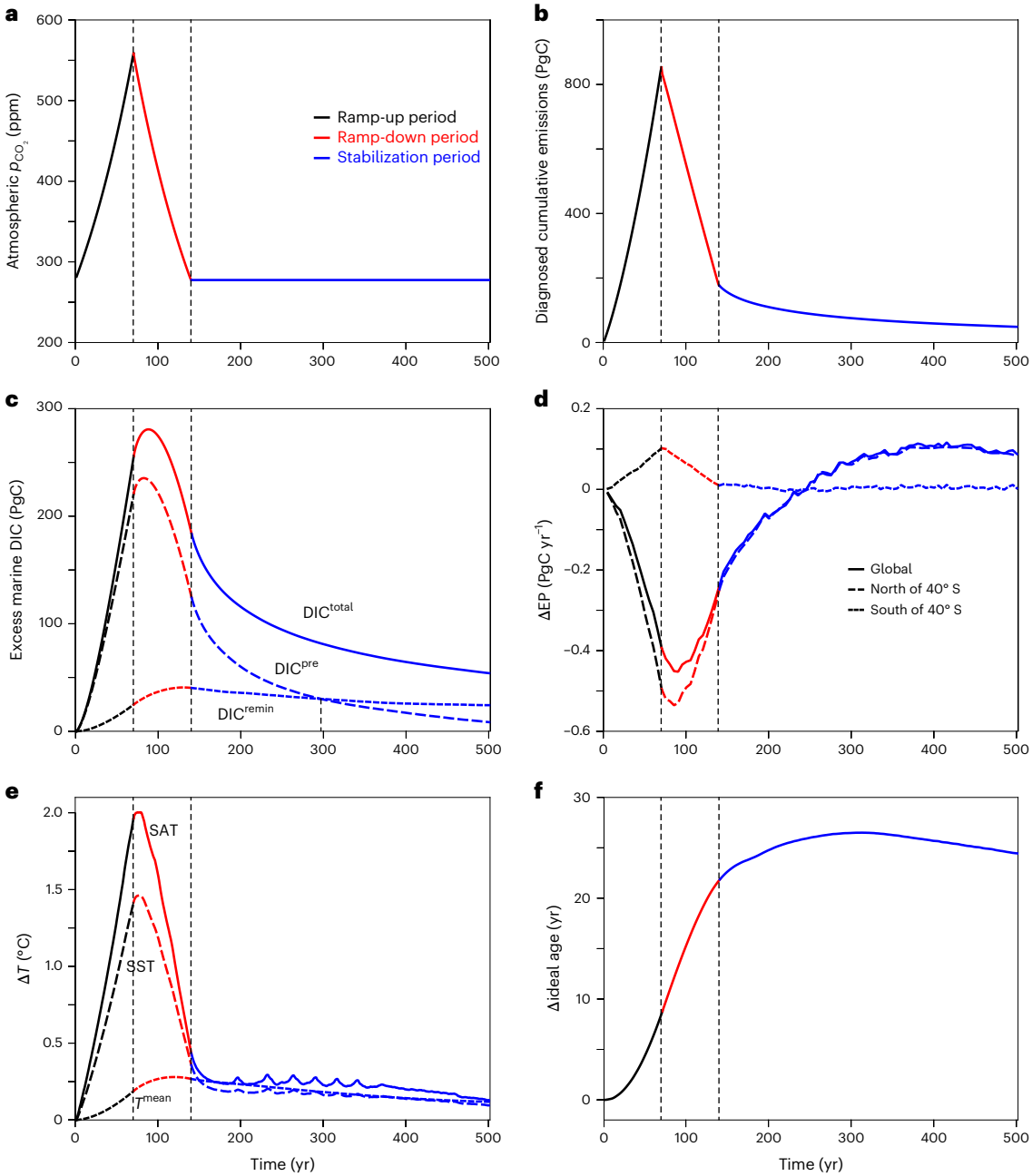


**Fig. 1 | Time evolution of global properties during the experiment REVERSE.** Results of default experiment REVERSE, where all changes in the ocean are relative to pre-industrial conditions. Throughout, black lines indicate the ramp-up period ($p_{CO_2}^{atm}$ increases), red lines denote the ramp-down period ($p_{CO_2}^{atm}$ decreases) and blue lines indicate the stabilization period with constant $p_{CO_2}^{atm}$ simulated until year 500. Vertical dashed lines at years 70 and 140 indicate the end of the ramp-up (peak $p_{CO_2}^{atm}$) and ramp-down periods, respectively. **a**, $p_{CO_2}^{atm}$ boundary condition. **b**, Diagnosed cumulative compatible emissions (measured in petagrams of carbon (PgC)). **c**, Globally integrated excess marine DIC (ΔDIC), which is excess total DIC ($DIC^{total}$, solid curve) with contributions from changes in preformed DIC ($DIC^{pre}$, dashed curve) and DIC attributable to the biological carbon pump ($DIC^{remin}$, dotted curve). The third vertical dashed line indicates the intersection point ($\Delta DIC^{remin} = \Delta DIC^{pre}$). **d**, Globally integrated excess export production (ΔEP, solid curve), ΔEP north of 40° S (dashed curve) and ΔEP south of 40° S (dotted curve). **e**, Change in temperature ($\Delta T$), which shows the variation in SAT (solid curve), variation in the sea surface temperature (SST, dashed curve) and variation in the ocean mean temperature ($T^{mean}$, dotted curve). **f**, Change in globally averaged ideal age (Δideal age).

Here we explored the contribution of biological-pump carbon to excess marine $CO_2$ storage ('excess' is used from now on to denote 'excess over the pre-industrial inventory') in idealized overshoot scenarios and on multi-centennial timescales using the University of Victoria (UVic) Earth system model of intermediate complexity (version 2.9). We defined biological-pump carbon as the part of dissolved inorganic carbon (DIC) that originates from biological processes (primary production, export flux and degradation of organic matter) and is stored in the ocean interior[13,17]. We found that, under scenarios which include periods of net-negative $CO_2$ emissions, excess $CO_2$ storage attributable to the biological carbon pump survived in the ocean over a considerably longer time compared with carbon stored due to physical–chemical processes (called 'solubility pump carbon' throughout; see 'Carbon pump terminology' in the Methods).

## Global excess DIC on multi-centennial timescales

We tested the stability of the marine carbon sink on the basis of an idealized overshoot scenario model experiment (see Methods for

details). In our default experiment, termed REVERSE (Fig. 1a), atmospheric $p_{CO_2}$ was prescribed to increase at 1% per year until reaching twice the pre-industrial $p_{CO_2}$ in year 70 (ramp-up phase), followed by a ramp-down phase with an equivalent drop in $p_{CO_2}^{atm}$ (that is, −1% per year) until pre-industrial levels are reached again in year 140; after this, there was a stabilization period characterized by a constant $p_{CO_2}$ until year 500. Compatible $CO_2$ emissions[25], consistent with this $p_{CO_2}^{atm}$ path, showed that cumulative negative emissions during the ramp-down phase were smaller compared with cumulative positive emissions during the ramp-up period (Fig. 1b).

This difference between the ramp-up and ramp-down cumulative emissions was explained by a considerable amount of carbon remaining in the ocean after $p_{CO_2}^{atm}$ had returned to pre-industrial levels (Fig. 1c, solid curve). By the end of the experiment, the marine carbon sink was mostly due to biological-pump carbon (Fig. 1c, dotted curve). We used idealized model tracers to attribute the contributions of individual marine carbon pumps to the excess in total DIC (ΔDIC) referenced to the pre-industrial state. Carbon processed by the biological carbon pump[7,26] was traced using an explicit tracer of remineralized DIC ($DIC^{remin}$). Briefly, the tracer is zero at the surface and accumulates $CO_2$ released during the remineralization of organic carbon in the ocean interior (see Methods for technical tracer definitions). Over the course of our 500 year experiment, this DIC component ($DIC^{remin}$) became an increasingly important contributor to ΔDIC (Fig. 1c and Supplementary Fig. 7b). At the end of the ramp-up period, the increase in $DIC^{remin}$ accounted for only about 10% (black portion of the dotted curve in Fig. 1c) of the integrated marine $CO_2$ uptake, whereas the change in preformed DIC ($DIC^{pre}$; black portion of the dashed curve in Fig. 1c) dominated the marine carbon sink. $DIC^{pre}$ is the DIC component that leaves the surface ocean as circulation occurs, that is, via advective transport and mixing. This component has no sinks or sources in the interior ocean. In our transient experiments, the increase in $DIC^{pre}$ was largely attributed to anthropogenic $CO_2$ entering the ocean, driven by the non-steady-state atmosphere–ocean $p_{CO_2}$ gradient (gas exchange) and enhanced by the buffer chemistry of $CO_2$ in seawater[27]. During and after the ramp-down period, however, $DIC^{pre}$ was rapidly lost from the ocean, simply because the atmosphere–ocean $p_{CO_2}$ gradient reversed due to a decrease in $p_{CO_2}^{atm}$ and circulation had not yet moved $DIC^{pre}$ far away from the surface layer. In addition to the reversal of the atmospheric $p_{CO_2}$ boundary condition, carbon–climate feedbacks, including the persistently warmer surface ocean, contributed to the loss of $DIC^{pre}$ (Supplementary Fig. 8). At the same time, $DIC^{remin}$ largely remained within the ocean and even increased its contribution to excess marine DIC over time (Fig. 1c and Supplementary Fig. 7b), accounting for about 22% at the end of the ramp-down period. After about 300 years into the model simulation, DIC attributable to the biological pump dominated ΔDIC in our default model experiment (Fig. 1c and Supplementary Fig. 7b).

## Spatial patterns of excess DIC storage

The timescales and pathways by which ΔDIC enters (and leaves) the ocean were reflected in the spatial and vertical distributions of excess $DIC^{pre}$ ($\Delta DIC^{pre}$) and excess $DIC^{remin}$ ($\Delta DIC^{remin}$) (Fig. 2). During the ramp-up phase, anthropogenic $CO_2$ entered the ocean essentially everywhere at the surface (Fig. 2a). Accordingly, the largest $\Delta DIC^{pre}$ was in the warm water sphere at the end of ramp-up period (Fig. 2a) as a consequence of the elevated pre-industrial surface ocean $CO_2$ buffer in warm low-latitude surface waters compared with cold high latitudes (Supplementary Fig. 1a, black line) and intensive ventiliation of intermediate and mode waters[2,28–31]. The former is consistent with the latitudinal distribution of the Revelle factor (for example, ref. 27). At the end of the ramp-down phase in year 140 (Fig. 2d), the 'bowl' of most elevated $\Delta DIC^{pre}$ (orange area in Fig. 2a) had disappeared whereas moderately elevated $\Delta DIC^{pre}$ had been transported southwards in the interior ocean with the flow of North Atlantic Deep Water and northwards with the flow of Antarctic Intermediate Water. Waters at the very surface, however, started to show negative $\Delta DIC^{pre}$ compared with the pre-industrial status, as a consequence of rapid equilibration with the atmosphere under conditions that were still warmer than pre-industrial sea surface temperatures (Fig. 1e; change in sea surface temperature (ΔSST) = 0.38 °C) and pre-industrial-like $p_{CO_2}^{atm}$ boundary conditions (Fig. 1a). By the end of our experiment in year 500, $\Delta DIC^{pre}$ in surface and deep waters had reduced further (Fig. 2g).

Spatial patterns of $\Delta DIC^{remin}$ developed quite differently compared with $\Delta DIC^{pre}$ over the course of experiment REVERSE. At peak $p_{CO_2}^{atm}$, $DIC^{remin}$ had changed little and in a patchy manner compared with the pre-industrial state ($\Delta DIC^{remin}$, Fig. 2b). Changes in $\Delta DIC^{remin}$ were only partly due to changes in net primary production (Supplementary Fig. 2) and export production (EP) (Fig. 1d), which can contribute to reducing $DIC^{remin}$ in low latitudes and increasing $DIC^{remin}$ in high latitudes[13]. However, globally integrated EP was lower than at pre-industrial times (black line in Fig. 1d) until year 250, and time-integrated excess EP (ΔEP) (not shown) remained negative even until the end of the experiment. Hence, the overall reduction in export carbon flux could not explain the overall increase in $\Delta DIC^{remin}$, consistent also with a recent climate model intercomparison study[17]. Both the global integral of $\Delta DIC^{remin}$ (Fig. 1c, dotted curve) and large-scale patterns of $\Delta DIC^{remin}$ (Fig. 2b) were dominated by the effect of increasing upper-ocean stratification and circulation changes on the accumulation time of organic matter degradation products in the interior ocean. We traced this change in accumulation time via changes in the ideal age (Δideal age; Figs. 1f and 2c). During the ramp-down period and until the end of the experiment (Fig. 2e,h), areas with lower than pre-industrial $DIC^{remin}$ became more prominent, particularly in the low latitudes. Here again, regions of decreasing $DIC^{remin}$ could not be explained by the time history of low-latitude EP observed in the experiment (Fig. 1d), but overall agreed better with patterns of reduced ideal age (Fig. 2f,i), indicating that a reduced accumulation time of $DIC^{remin}$ was a major source of regional lows in $\Delta DIC^{remin}$. In turn, larger ideal ages in the Southern Ocean and the deep ocean, developing already during the ramp-up phase and strengthening during the ramp-down phase (Fig. 2c,f), indicated a prolonged accumulation time of $DIC^{remin}$ together with reduced outgassing with increasing stratification as major causes of regional highs in $\Delta DIC^{remin}$ (Fig. 2b,e). In addition, elevated $DIC^{remin}$ and ideal age changes originating to a large part in the Southern Ocean (Fig. 2b,e and Fig. 2c,f, respectively) were later transported into deep and bottom waters of the Atlantic and Pacific Oceans (Fig. 2h) and were also subject to mixing. Given the millennial-timescale residence times (that is, the time until re-emergence at the surface) of these waters[32], we speculate that the slow rate of decrease of globally integrated $\Delta DIC^{remin}$ observed until year 500 (Fig. 1c) may persist for an even longer time as elevated $\Delta DIC^{remin}$ was trapped in the deep-ocean circulation.

We confirmed the results of REVERSE in experiments with modified model variants and modified $p_{CO_2}^{atm}$ trajectories, which differ by the speed of $p_{CO_2}$ decrease after year 70 (Supplementary Figs. 3 and 4), and found that $\Delta DIC^{remin}$ was more durable than $\Delta DIC^{pre}$ and became the dominant marine storage of excess $CO_2$ (ΔDIC) on multi-centennial timescales in most of the studied scenarios (see Supplementary Results for details).

## The marine carbon sink under moderate overshoot scenarios

As a return to pre-industrial $p_{CO_2}^{atm}$ in experiment REVERSE implies an ambitious mitigation pathway, we also explored the response of ocean carbon storage and the relative importance of biological-pump carbon ($DIC^{remin}$) and solubility-pump carbon ($DIC^{pre}$) via—according to current ambitions—more realistic moderate overshoot scenarios that return to the 1.5 °C target after shortly passing a warming of 2 °C. We explored a moderate SAT overshoot as a consequence of delayed $CO_2$ emission reduction efforts for idealized experiments in which anthropogenic net-zero emissions were assumed around the ΔSAT = 1.5 °C climate

https://doi.org/10.1038/s41561-024-01541-y

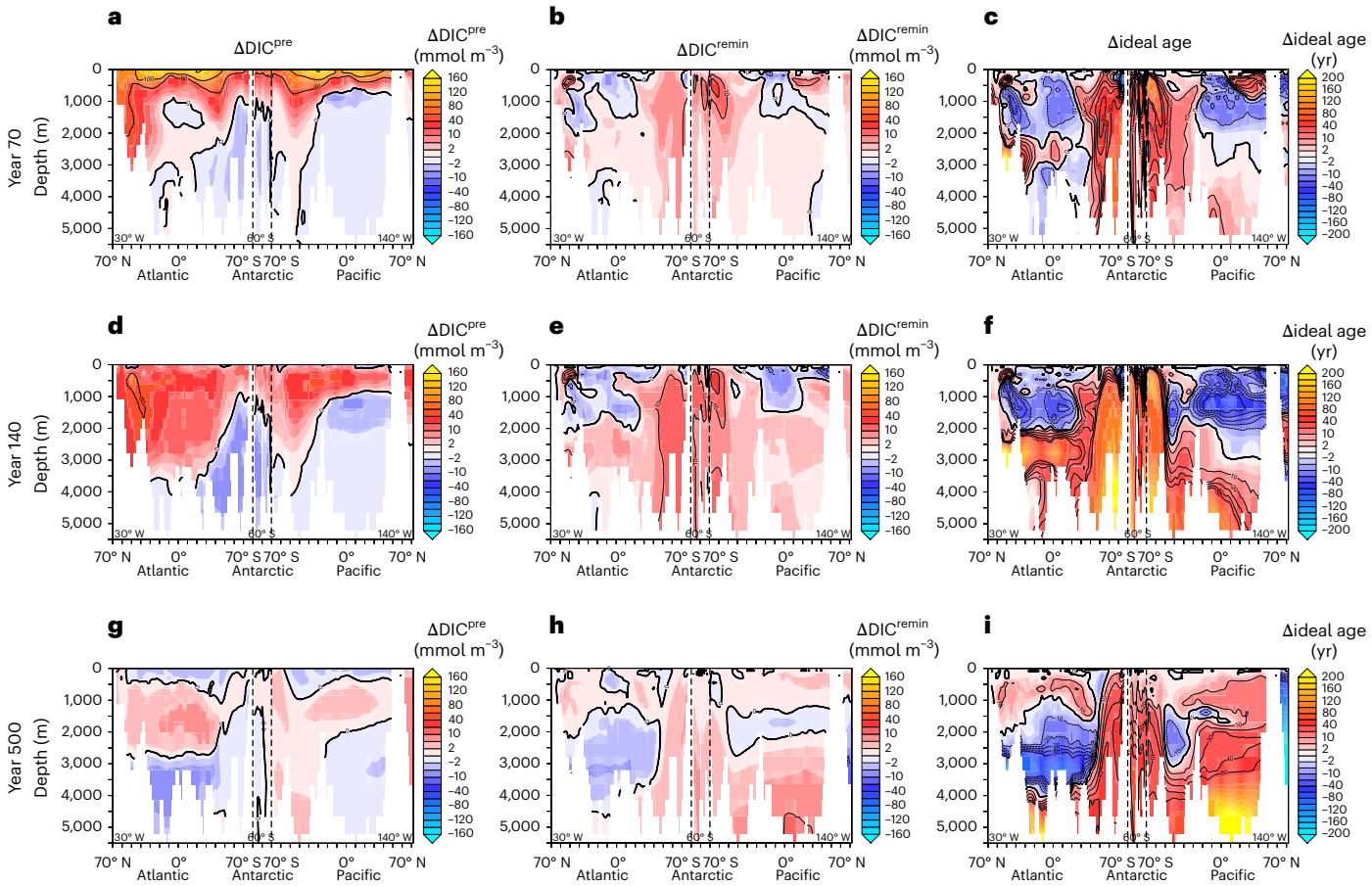


**Fig. 2 | Vertical distribution of ΔDIC$^{pre}$, ΔDIC$^{remin}$ and Δideal age. a–i**, For experiment REVERSE, ocean sections of ΔDIC$^{pre}$ (**a**,**d**,**g**), ΔDIC$^{remin}$ (**b**,**e**,**h**) and Δideal age (**c**,**f**,**i**) at the end of the ramp-up period (year 70, **a**–**c**), the end of the ramp-down period (year 140, **d**–**f**) and at year 500 (**g**–**i**). Changes relative to pre-industrial levels (for example, year 70 − pre-industrial) are shown. Running from left to right in each plot, the *x* axes show distributions along 30° W (from north to south) in the Atlantic Ocean, in the Southern Ocean (at 60° S, from east to west) and in the Pacific Ocean (140° W, from south to north).

target after passing the maximum temperature in experiment REVERSE (for which ΔSAT = 2.02 °C) (see details in Supplementary Methods). All experiments branching off from experiment REVERSE with net-zero emissions showed a slow long-term decline in SAT (Fig. 3a; ~0.04 °C per 100 years) and an associated decline in atmospheric $p_{CO_2}$ (Fig. 3b), consistent with anthropogenic net-zero emissions and the slow continued uptake of $CO_2$ and heat by the ocean. ΔDIC$^{remin}$ (Fig. 3d) increased continuously until the end of the experiments. This prominent increase in ΔDIC$^{remin}$ was explained by continuous ocean heat uptake (Fig. 3e, coloured lines). This continuous ocean heat uptake prolonged the conditions of elevated upper-ocean temperature gradients (Fig. 3f), which through their effect on the vertical density structure supported isolation of the interior ocean as indicated by a continuous increase in the global ideal age anomaly (Fig. 3g). ΔDIC$^{remin}$ (relative to pre-industrial conditions; Fig. 3d, coloured lines) never exceeded ΔDIC$^{pre}$ (Fig. 3c). However, computing ΔDIC components relative to the time point after which we assumed net-zero $CO_2$ emissions (vertical dashed lines in Fig. 3) changed the picture. In the overshoot experiments, ΔDIC$^{remin}$ computed this way (solid orange curve in Fig. 3h) was much larger compared with the equivalent ΔDIC$^{pre}$ (dashed orange curve in Fig. 3h). In other words, biological-pump carbon dominated additional $CO_2$ storage after a moderate temperature overshoot. For net-zero $CO_2$ emission experiments without any temperature and $p_{CO_2}$ overshoot, this was not observed (green curves in Fig. 3h)—that is, DIC$^{pre}$ (solubility-pump carbon) remained the major marine carbon sink under the conditions of net-zero emissions and climate stabilization without temperature and $p_{CO_2}$ overshoot.

We suggest that the differences in ΔDIC$^{pre}$ for experiments with and without $p_{CO_2}$ and temperature overshoot can be understood in terms of a delayed response to the time history of atmospheric $p_{CO_2}$. Assuming that the physico-chemical uptake of atmospheric $CO_2$ by the ocean (into DIC$^{pre}$) responds to negative $CO_2$ emissions with a similar impulse response function[33] as it does to positive emissions, we suggest that the negative emissions between peak $p_{CO_2}$ and net-zero emission regimes caused a stronger loss of DIC$^{pre}$ (dashed orange line) compared with the simulation without net-negative emissions (dashed green line).

## Potential implications for integrated assessment modelling

With the ocean being a principal player in the global carbon cycle and for the uptake of anthropogenic $CO_2$ (refs. 34,35), recent efforts have focused on better understanding the impact of climate change on the marine uptake of anthropogenic $CO_2$, for example, by weakening the overturning circulation and the effect of climate change on the natural marine carbon cycle, both under scenarios of increasing $CO_2$ emissions[5,36,37]. However, the response and relative importance of the marine carbon–climate and carbon–concentration feedbacks under scenarios of net-negative (or net-zero) $CO_2$ emissions remain unknown. Here we showed that, under scenarios of net-negative $CO_2$ emissions, the ocean may become a source of formerly stored anthropogenic $CO_2$ to the atmosphere, while additional $CO_2$ stored in the ocean and attributable to the biological pump outgassed from the ocean at a much slower rate and became an important component of centennial-timescale marine carbon storage. Acknowledging the

https://doi.org/10.1038/s41561-024-01541-y

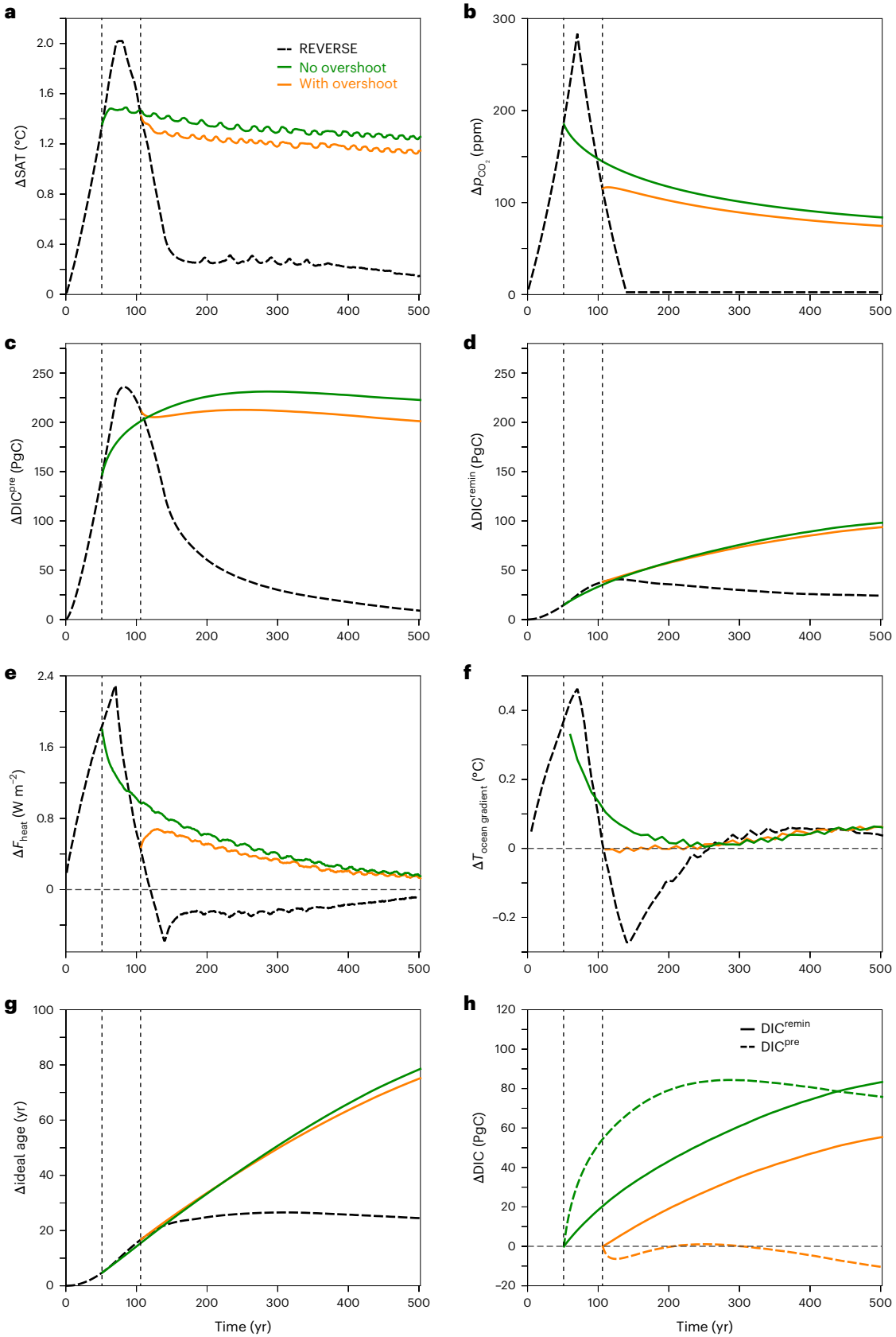


**Fig. 3 | Time evolution of global properties after moderate temperature overshoot. a**–**h**, Model projections with anthropogenic net-zero $CO_2$ emissions starting close to the +1.5 °C climate target for ΔSAT are shown. ΔSAT (**a**), $\Delta p_{CO_2}^{atm}$ (**b**), $\Delta DIC^{pre}$ (**c**), $\Delta DIC^{remin}$ (**d**), heat flux ($\Delta F_{heat}$) (**e**), vertical temperature gradient in the upper ocean (upper 200 m) (**f**), Δideal age (**g**) and $\Delta DIC^{remin}$ (solid coloured lines) and $\Delta DIC^{pre}$ (dashed coloured lines) relative to branching-off values (**h**). Experiments branch off from REVERSE either after a moderate temperature overshoot (orange curves) or when reaching the climate target for the first time (green curves). The REVERSE results (dashed black curves) are shown for reference. Anomalies relative to pre-industrial conditions (**a**–**g**) or relative to the branching-off state (**h**) of global means (**a**,**b**,**e**–**g**) and inventories (**c**,**d**,**h**) are shown.

simplicity of our Earth system model and the ideality of our experiments, we expect our main conclusion to hold for simulations with more complex Earth system models and more realistic emissions scenarios, as supported by our various sensitivity-model experiments.

This shift in processes relevant for marine $CO_2$ storage under net-negative emissions has so far not been recognized. It is of particular relevance in the context of the socio-economic evaluation of potential future emission and climate pathways as the class of models used there (integrated assessment models, or IAMs) utilize simple climate models such as MAGICC (Model for the Assessment of Greenhouse Gas Induced Climate Change)[38], which typically represent the marine carbon sink via an impulse response function (see, for example, ref. 33), assuming a purely physico-chemical behaviour of $CO_2$ uptake. As these models are usually trained against Earth system model output from experiments similar to our ramp-up phase, they do not represent the fact that Earth system feedbacks like the storage via biological-pump carbon become increasingly relevant after a temperature overshoot and subsequent net-negative emissions. We speculate that the lack of representation of this feedback may cause an underestimation of the marine carbon sink and an overestimation of the eventually needed net-negative emissions. In agreement with ref. 39, we propose that a better integration of such Earth system feedbacks may be needed to realistically project the centennial-timescale future of marine $CO_2$ uptake and storage under complex emission scenarios, and benefit more realistic climate mitigation scenarios.

## Online content

Any methods, additional references, Nature Portfolio reporting summaries, source data, extended data, supplementary information, acknowledgements, peer review information; details of author contributions and competing interests; and statements of data and code availability are available at https://doi.org/10.1038/s41561-024-01541-y.

## References


1. Friedlingstein, P. et al. Global carbon budget 2022. *Earth Syst. Sci. Data* **14**, 4811–4900 (2022).
2. Gruber, N. et al. The oceanic sink for anthropogenic $CO_2$ from 1994 to 2007. *Science* **363**, 1193–1199 (2019).
3. Gruber, N. et al. Trends and variability in the ocean carbon sink. *Nat. Rev. Earth Environ.* **4**, 119–134 (2023).
4. Dunne, J. P. Physical mechanisms driving enhanced carbon sequestration by the biological pump under climate warming. *Global Biogeochem. Cycles* **37**, e2023GB007859 (2023).
5. Arora, V. K. et al. Carbon-concentration and carbon-climate feedbacks in CMIP6 models and their comparison to CMIP5 models. *Biogeosciences* **17**, 4173–4222 (2020).
6. Bernardello, R. et al. Response of the ocean natural carbon storage to projected twenty-first-century climate change. *J. Clim.* **27**, 2033–2053 (2014).
7. Volk, T. & Hoffert, M. I. Ocean carbon pumps: analysis of relative strengths and efficiencies in ocean-driven atmospheric $CO_2$ changes. In *The Carbon Cycle and Atmospheric $CO_2$: Natural Variations Archean to Present* (eds Sundquist, E. T. & Broecker, W. S.) 99–110 (American Geophysical Union, 1985).
8. Carroll, D. et al. Attribution of space-time variability in global-ocean dissolved inorganic carbon. *Global Biogeochem. Cycles* **36**, e2021GB007162 (2022).
9. Galbraith, E. D. & Skinner, L. C. The biological pump during the Last Glacial Maximum. *Ann. Rev. Mar. Sci.* **12**, 559–586 (2020).
10. Cabré, A., Marinov, I. & Leung, S. Consistent global responses of marine ecosystems to future climate change across the IPCC AR5 earth system models. *Clim. Dyn.* **45**, 1253–1280 (2015).
11. Laufkötter, C. et al. Drivers and uncertainties of future global marine primary production in marine ecosystem models. *Biogeosciences* **12**, 6955–6984 (2015).
12. Laufkötter, C. et al. Projected decreases in future marine export production: the role of the carbon flux through the upper ocean ecosystem. *Biogeosciences* **13**, 4023–4047 (2016).
13. Koeve, W., Kähler, P. & Oschlies, A. Does export production measure transient changes of the biological carbon pump's feedback to the atmosphere under global warming? *Geophys. Res. Lett.* **47**, e2020GL089928 (2020).
14. Ito, T. et al. Sustained growth of the Southern Ocean carbon storage in a warming climate. *Geophys. Res. Lett.* **42**, 4516–4522 (2015).
15. Bernardello, R., Marinov, I., Palter, J. B., Galbraith, E. D. & Sarmiento, J. L. Impact of Weddell Sea deep convection on natural and anthropogenic carbon in a climate model. *Geophys. Res. Lett.* **41**, 7262–7269 (2014).
16. Frenger, I. et al. Misconceptions of the marine biological carbon pump in a changing climate: thinking outside the "export" box. *Glob. Change Biol.* **30**, e17124 (2024).
17. Wilson, J. D. et al. The biological carbon pump in CMIP6 models: 21st century trends and uncertainties. *Proc. Natl Acad. Sci. USA* **119**, e2204369119 (2022).
18. *Paris Agreement* (UNFCCC, 2015).
19. Rogelj, J. et al. in *Special Report on Global Warming of 1.5 °C* (eds Masson-Delmotte, V. et al.) 93–174 (IPPC, Cambridge Univ. Press, 2018).
20. Fuss, S. et al. Research priorities for negative emissions. *Environ. Res. Lett.* **11**, 115007 (2016).
21. Zickfeld, K., MacDougall, A. H. & Matthews, H. D. On the proportionality between global temperature change and cumulative $CO_2$ emissions during periods of net negative $CO_2$ emissions. *Environ. Res. Lett.* **11**, 055006 (2016).
22. Melnikova, I. et al. Carbon cycle response to temperature overshoot beyond 2 °C: an analysis of CMIP6 models. *Earths Future* **9**, e2020EF001967 (2021).
23. Asaadi, A. et al. Carbon cycle feedbacks in an idealized simulation and a scenario simulation of negative emissions in CMIP6 Earth system models. *Biogeosciences* **21**, 411–435 (2024).
24. Li, X. R., Zickfeld, K., Mathesius, S., Kohfeld, K. & Matthews, J. B. R. Irreversibility of marine climate change impacts under carbon dioxide removal. *Geophys. Res. Lett.* **47**, e2020GL088507 (2020).
25. Jones, C. et al. Twenty-first-century compatible $CO_2$ emissions and airborne fraction simulated by CMIP5 Earth system models under four representative concentration pathways. *J. Clim.* **26**, 4398–4413 (2013).
26. Shaffer, G. Effects of the marine biota on global carbon cycling. In *The Global Carbon Cycle* (ed. Heimann, M.) 431–455 (Springer, 1993).
27. Jiang, L.-Q., Carter, B. R., Feely, R. A., Lauvset, S. K. & Olsen, A. Surface ocean pH and buffer capacity: past, present and future. *Sci. Rep.* **9**, 18624 (2019).
28. Sallée, J. B. et al. Assessment of Southern Ocean water mass circulation and characteristics in CMIP5 models: historical bias and forcing response. *J. Geophys. Res. Oceans* **118**, 1830–1844 (2013).
29. Sabine, C. L. et al. The oceanic sink for anthropogenic $CO_2$. *Science* **305**, 367–371 (2004).
30. Resplandy, L., Bopp, L., Orr, J. C. & Dunne, J. P. Role of mode and intermediate waters in future ocean acidification: analysis of CMIP5 models. *Geophys. Res. Lett.* **40**, 3091–3095 (2013).
31. Hong, Y. et al. Subantarctic mode water and its long-term change in CMIP6 models. *J. Clim.* **34**, 9385–9400 (2021).
32. DeVries, T., Primeau, F. & Deutsch, C. The sequestration efficiency of the biological pump. *Geophys. Res. Lett.* **39**, L13601 (2012).
33. Joos, F. et al. Carbon dioxide and climate impulse response functions for the computation of greenhouse gas metrics: a multi-model analysis. *Atmos. Chem. Phys.* **13**, 2793–2825 (2013).

34. Friedlingstein, P. et al. Global carbon budget 2020. *Earth Syst. Sci. Data* **12**, 3269–3340 (2020).
35. McKinley, G. A., Fay, A. R., Lovenduski, N. S. & Pilcher, D. J. Natural variability and anthropogenic trends in the ocean carbon sink. *Ann. Rev. Mar. Sci.* **9**, 125–150 (2017).
36. Matear, R. J. & Hirst, A. C. Climate change feedback on the future oceanic $CO_2$ uptake. *Tellus B Chem. Phys. Meteorol.* **51**, 722–733 (1999).
37. Holzer, M., Chamberlain, M. A. & Matear, R. J. Climate-driven changes in the ocean's ventilation pathways and time scales diagnosed from transport matrices. *J. Geophys. Res. Oceans* **125**, e2020JC016414 (2020).
38. Meinshausen, M., Raper, S. C. B. & Wigley, T. M. L. Emulating coupled atmosphere-ocean and carbon cycle models with a simpler model, MAGICC6 – part 1: model description and calibration. *Atmos. Chem. Phys.* **11**, 1417–1456 (2011).
39. Rickels, W. & Schwinger, J. Implications of temperature overshoot dynamics for climate and carbon dioxide removal policies in the DICE model. *Environ. Res. Lett.* **16**, 104042 (2021).

## Methods

We used a modified version of the UVic Earth system model of intermediate complexity (version 2.9)[40,41], which we ran in an ocean–atmosphere–sea-ice configuration[13]. The ocean biogeochemistry used in this model was based on an NPZD model—which simulates interactions between the model compartments' nutrients (N), phytoplankton (P), zooplankton (Z) and detritus (D)—with phosphate and nitrate as prognostic nutrients and iron limitation prescribed by an iron concentration mask[42]. The model simulated diazotrophs and ordinary phytoplankton, one zooplankton and one detritus pool. It applied fixed elemental ratios (of C:N:P:$O_2$) for organic matter cycling and the interactions with prognostic oxygen, total DIC and alkalinity tracers. The degradation of organic matter was temperature-sensitive. For more details on model equations and evaluation against observations, see ref. 42.

### DIC component attribution

We used idealized model tracers to distinguish the contributions from different processes to total DIC[6]. $DIC^{remin}$ represented the impact of organic matter degradation on DIC in the interior ocean. Below the surface layer (that is, below $z = 50$ m in this model), $DIC^{remin}$ was subject to source-minus-sink terms associated with organic matter degradation (and production). In the surface layer, $DIC^{remin}$ was set to zero at any time step during the model run time. $DIC^{pre}$ represented the fraction of DIC that behaves conservatively in the ocean. At the surface, $DIC^{pre}$ was set to the value of DIC; in the interior ocean it had no biogeochemical sinks or sources. Implicitly, $DIC^{pre}$ was also affected by gas exchange, and hence by the transient changes in atmospheric $CO_2$ in the experiments performed here (see below). In the interior ocean ($z > 50$ m), both tracers (as with any other tracer) were transported according to the model physics and could be (further) modified due to the mixing of water masses. A third component, the DIC affected by the production or dissolution of $CaCO_3$, was not modelled explicitly but may be computed via difference between DIC and $DIC^{remin} + DIC^{pre}$. In this study we particularly reported and analysed changes in $DIC^{pre}$ and $DIC^{remin}$. In a climate change context, $DIC^{pre}$ increases when anthropogenic $CO_2$ enters the ocean; $DIC^{pre}$ can also change as a consequence of carbon–climate feedbacks[6] (Supplementary Methods and Supplementary Fig. 8). The former process, however, dominated the change in $DIC^{pre}$ in particular during the ramp-up phase. $DIC^{remin}$ was subject to carbon–climate feedbacks, for example, by changing circulation (changing the residence time of the interior-ocean water) or changing the export flux of organic matter. Our model did not include $CO_2$–concentration feedbacks on biology, assuming that $CO_2$ is never limiting for biological growth in marine surface waters. In other words, we assumed no effects of ocean acidification on phytoplankton.

We further applied an ideal age tracer[43,44]. An ideal age tracer quantifies the mean age since last contact with the atmosphere. This tracer was set to zero at the surface of the ocean and ages at a rate of one day per day everywhere else. The tracer was also subject to physical transports and water-mass mixing. We note that an ideal age tracer is an ideal tracer of mean age in the steady state. Tracers of the model's true oxygen utilization (or TOU) and preformed oxygen ($O_2^{pre}$) were defined as analogues of $DIC^{remin}$ and $DIC^{pre}$, respectively, with respect to their sink and source terms and surface ocean boundary conditions[45].

### Default model experiment

The experiment presented here was based on a 10,000-year-long experiments run with prescribed constant pre-industrial $pCO_2$ and climate forcing (spinup) with the fully coupled model, followed by 1,500 years with the ocean–atmosphere–sea-ice model (see ref. 13 for details and model evaluation). Using an ocean–atmosphere–sea-ice model with idealized $p_{CO_2}$ concentration forcing, we neglected any non-$CO_2$ forcings and feedbacks. We performed idealized $CO_2$- and temperature-overshoot experiments (experiment REVERSE, modified from 'CDR-reversibility' experiments described in ref. 46) starting at pre-industrial conditions with a 1% increase in atmospheric $p_{CO_2}$ per year until twice the pre-industrial $CO_2$ conditions were reached (ramp-up phase, 70 years). Thereafter, atmospheric $p_{CO_2}$ was predicted to decrease at a rate of −1% per year until pre-industrial $p_{CO_2}$ was reached again (ramp-down phase, years 71–140). The experiment was continued until year 500 with predicted pre-industrial $p_{CO_2^{atm}}$ (stabilization phase, years 141–500).

### Sensitivity experiments

To demonstrate the robustness of our main findings, we carried out idealized sensitivity experiments with different model set-ups (circulation strength and biogeochemistry), modified assumptions about negative emissions during ramp-down and different peak $p_{CO_2^{atm}}$ conditions. Further sensitivity experiments performed using the default model set-up explored potential effects concerning the predicted $p_{CO_2^{atm}}$ rate of decrease after peak $p_{CO_2}$, that is, assuming a slower $p_{CO_2^{atm}}$ decrease. We also performed experiments with a moderate temperature overshoot. All sensitivity experiments were run for 500 years in total. Details of the sensitivity experiments are given in the Supplementary Information.

### Compatible $CO_2$ emissions

In an Earth system model experiment with prescribed $p_{CO_2^{atm}}$, compatible emissions (emissions consistent with this atmospheric $p_{CO_2}$ path and the models Earth System feedbacks) were diagnosed from the change in the Earth system carbon inventory (land + ocean + atmospheric carbon) relative to the pre-industrial state[25]. Carbon–climate feedbacks, such as the warming $CO_2$-solubility feedback, reduced the compatible emissions by reducing the marine carbon sink (reducing $DIC^{pre}$). For the applied ocean–atmosphere–sea-ice model, land carbon change was not considered in the computation of compatible emissions.

### Carbon pump terminology

Processes that give rise to a vertical gradient of DIC in the ocean and thereby affect $p_{CO_2^{atm}}$ have been referred to as marine carbon pumps[7]. Since the original proposal of the three pumps (soft-tissue pump, $CaCO_3$ pump and solubility pump), they have been addressed using slightly differing terminologies in the literature. Here we adopt, for example, from ref. 47 and others, usage of the generic term 'biological (carbon) pump' for what originally was more specifically referred to as the 'soft tissue pump' by Volk and Hoffert[7]. This carbon pump starts with the incorporation of $CO_2$ into living organic matter (tissue) by phytoplankton, followed by organic carbon propagating through the food web and eventually being transported into the interior ocean (via sinking particles, active transport and physical mixing; see, for example, ref. 48). In the interior ocean the majority of organic matter is degraded back to $CO_2$, entering the pool of total DIC, and nutrients, with a small fraction sinking down to the sediment. The degradation products are subject to transport by the ocean's circulation. The amount of DIC attributable to the soft-tissue pump that we trace with our idealized model tracer $DIC^{remin}$ in the interior ocean is due to the balance of processes that increase $DIC^{remin}$ (organic matter transport and subsequent degradation in the ocean interior) and ocean circulation, which will return the degradation products to the surface ocean (see ref. 16 for a more detailed discussion). The soft-tissue pump is considered to be the dominant biological pathway for enhancing DIC in the interior ocean[49,50], and has a considerable long-term impact on atmospheric $p_{CO_2}$ (ref. 51). The $CaCO_3$ (counter) pump, the second biological carbon pump defined in ref. 7, is not traced by $DIC^{remin}$, nor can it meaningfully be traced by an idealized carbon tracer as the $CaCO_3$ pump is primarily an alkalinity pump (exporting alkalinity and DIC into the deep ocean in a 2:1 ratio) and hence has an inverse effect on marine carbon storage. In this context, we note that changes in $DIC^{remin}$ and $DIC^{pre}$ do not perfectly add up to changes in DIC ($\Delta DIC \neq \Delta DIC^{remin} + \Delta DIC^{pre}$). This is so because DIC that is attributable to the

$CaCO_3$ pump (that is, $\Delta DIC^{ca}$) may change as well. In the experiment REVERSE, the globally integrated residual ($\Delta DIC - \Delta DIC^{pre} - \Delta DIC^{remin} = \Delta DIC^{ca}$) was 9.7 PgC (4% of ΔDIC) at peak $p_{CO_2}$, 19 PgC (10% of ΔDIC) in year 140 and 21.5 PgC (26%) at the intersection point ($\Delta DIC^{remin} = \Delta DIC^{pre}$). We note that this increase in $DIC^{ca}$ (Supplementary Fig. 7) does not contribute to an increase in the ocean carbon sink as the $CaCO_3$ pump is inevitably linked to a decrease in surface alkalinity, contributing to the decrease in $DIC^{pre}$ from carbon–climate feedbacks (see Supplementary Fig. 8) to a so far unquantified degree. The majority of marine DIC is $DIC^{pre}$, which is a consequence of the $CO_2$ buffer chemistry of seawater and the associated solubility of $CO_2$ in equilibrium with the atmosphere. The original term 'solubility pump'[7] addressed the contribution of high-to-low-latitude temperature gradients together with the large-scale overturning circulation on the vertical DIC gradient, leaving the huge background DIC unnamed. At pre-industrial times, $DIC^{pre}$ includes both this background DIC and the DIC explicitly related to the solubility pump according to Volk and Hoffert[7]. Acknowledging that the physical–chemical marine uptake of anthropogenic $CO_2$ is controlled by $CO_2$ buffer chemistry and solubility, next to the partial pressure gradient and the circulation, we use the term solubility-pump carbon as a synonym for $DIC^{pre}$.

## Data availability

Model output is available from GEOMAR at https://hdl.handle.net/20.500.12085/959a266e-d785-4d57-87bb-103b28d2bb25.

## Code availability

Model code is available from GEOMAR at https://hdl.handle.net/20.500.12085/959a266e-d785-4d57-87bb-103b28d2bb25.

## References


40. Eby, M. et al. Historical and idealized climate model experiments: an intercomparison of Earth system models of intermediate complexity. *Clim. Past* **9**, 1111–1140 (2013).
41. Weaver, A. J. et al. The UVic earth system climate model: model description, climatology, and applications to past, present and future climates. *Atmos. Ocean* **39**, 361–428 (2001).
42. Keller, D. P., Oschlies, A. & Eby, M. A new marine ecosystem model for the University of Victoria Earth System Climate Model. *Geosci. Model Dev.* **5**, 1195–1220 (2012).
43. England, M. H. The age of water and ventilation timescales in a global ocean model. *J. Phys. Oceanogr.* **25**, 2756–2777 (1995).
44. Koeve, W., Wagner, H., Kähler, P. & Oschlies, A. $^{14}C$-age tracers in global ocean circulation models. *Geosci. Model Dev.* **8**, 2079–2094 (2015).
45. Koeve, W. & Kähler, P. Oxygen utilization rate (OUR) underestimates ocean respiration: a model study. *Global Biogeochem. Cycles* **30**, 1166–1182 (2016).
46. Keller, D. P. et al. The Carbon Dioxide Removal Model Intercomparison Project (CDRMIP): rationale and experimental protocol for CMIP6. *Geosci. Model Dev.* **11**, 1133–1160 (2018).
47. De La Rocha, C. L. & Passow, U. Factors influencing the sinking of POC and the efficiency of the biological carbon pump. *Deep Sea Res. 2 Top. Stud. Oceanogr.* **54**, 639–658 (2007).
48. Boyd, P. W., Claustre, H., Levy, M., Siegel, D. A. & Weber, T. Multi-faceted particle pumps drive carbon sequestration in the ocean. *Nature* **568**, 327–335 (2019).
49. Sarmiento, J. L. & Gruber, N. *Ocean Biogeochemical Dynamics* (Princeton Univ. Press, 2006).
50. Oka, A. Ocean carbon pump decomposition and its application to CMIP5 earth system model simulations. *Prog. Earth Planet Sci.* **7**, 25 (2020).
51. Kwon, E. Y., Sarmiento, J. L., Toggweiler, J. R. & DeVries, T. The control of atmospheric $pCO_2$ by ocean ventilation change: the effect of the oceanic storage of biogenic carbon. *Global Biogeochem. Cycles* **25**, GB3026 (2011).


## Acknowledgements


We thank colleagues from the Biogeochemical Modelling unit at GEOMAR, in particular members of the 'Biological Pump Pathfinder Group', for discussions. K. Kvale (Institute of Geological and Nuclear Sciences, New Zealand), H. Guo and W. (Ben) Yao (both GEOMAR, Germany) provided comments on earlier versions of our manuscript. We thank E. Monteiro (GEOMAR, Germany) and D. P. Keller (now at the Carbon to Sea Initiative, https://carbontosea.org/) for discussing with us their unpublished results from CDRMIP. This research was supported in part through high-performance computing resources available at the Kiel University Computing Centre. We wish to acknowledge use of the Ferret program for analysis and graphics in this paper. Ferret is a product of the NOAA Pacific Marine Environmental Laboratory (information is available at http://ferret.pmel.noaa.gov/Ferret/). We acknowledge funding by the European Union (ERC, OSTIA, 101116545; to I.F.). This work is a contribution to the GEOMAR POF IV program 'Changing Earth – Sustaining our Future, Topic 6.3: The Future Biological Carbon Pump'.


## Author contributions

W.K. designed the research and performed the model experiments. W.K. and I.F. analysed the model output. W.K. wrote the first draught of the paper, and A.L., A.O. and I.F. discussed the draught and contributed to the writing of the paper.

## Funding


Open access funding provided by GEOMAR Helmholtz-Zentrum für Ozeanforschung Kiel.


## Competing interests

The authors declare no competing interests.

## Additional information

**Supplementary information** The online version contains supplementary material available at https://doi.org/10.1038/s41561-024-01541-y.


**Correspondence and requests for materials** should be addressed to Wolfgang Koeve or Ivy Frenger.



**Peer review information** *Nature Geoscience* thanks Xinru Li, Jamie Wilson and the other, anonymous, reviewer(s) for their contribution to the peer review of this work. Primary Handling Editor: Tom Richardson, in collaboration with the *Nature Geoscience* team.